Molecular Pharmacology Fast Forward. Published on November 26, 2019 as DOI: 10.1124/mol.119.117549
This article has not been copyedited and formatted. The final version may differ from this version.

MOL Manuscript # 117549

Characterization and optimization of the novel TRPM2 antagonist tatM2NX

Cruz-Torres, I.; Backos, D.S.; and Herson, P.S.

Department of Pharmacology, University of Colorado School of Medicine, Aurora, CO, USA (I.C.T, P.S.H.)

Department of Pharmaceutical Sciences, University of Colorado Skaggs School of Pharmacy and Pharmaceutical Sciences, Aurora, CO, USA (D.S.B.)

Department of Anesthesiology, University of Colorado School of Medicine, Aurora, CO, USA (P.S.H.)

Neuronal Injury & Plasticity Program, University of Colorado School of Medicine, Aurora, CO, USA (I.C.T, P.S.H.)

Corresponding author: Ivelisse Cruz-Torres (ivelisse.cruz-torres@ucdenver.edu), Paco S. Herson (paco.herson@ucdenver.edu); telephone: 303-724-6628; fax: 303-724-1761

Address: Department of Pharmacology, University of Colorado School of Medicine, Aurora, CO, USA

Molecular Pharmacology Fast Forward. Published on November 26, 2019 as DOI: 10.1124/mol.119.117549
This article has not been copyedited and formatted. The final version may differ from this version.

MOL Manuscript # 117549

Running title: Characterization of the TRPM2 antagonist tatM2NX

Number of text pages: 32

Number of tables: 2

Number of figures: 4

Number of references: 75

Number of words abstract: 171

Number of words introduction: 667

Number of words discussion: 1086

Abbreviations: adenosine diphosphate ribose**,** ADPR; clotrimazole, CTZ; cryo-electron miscroscopy, cryoEM; doxycycline, Dox; Nudix Hydrolase 9 homology domain, NUDT9-H; structure-activity relationship, SAR; transient receptor potential melastatin 2, TRPM2; calcium, Ca^{2+}; hydrogen peroxide, H_2O_2; N-terminus, Nterm; C-terminus, Cterm; IC_{50}, half maximal inhibitory concentration; nanoseconds, ns; molecular dynamics, MD.

Keywords: human TRPM2 channels, peptide antagonist, tatM2NX, structure-activity relationship

Molecular Pharmacology Fast Forward. Published on November 26, 2019 as DOI: 10.1124/mol.119.117549
This article has not been copyedited and formatted. The final version may differ from this version.

Abstract

TRPM2 is a calcium permeable channel activated by ADPR metabolites and oxidative stress. TRPM2 contributes to neuronal injury in the brain caused by stroke and cardiac arrest among other diseases including pain, inflammation, and cancer. However, the lack of specific inhibitors hinders the study of TRPM2 in brain pathophysiology. Here we present the design of a novel TRPM2 antagonist, tatM2NX, which prevents ligand binding and TRPM2 activation. We used mutagenesis of tatM2NX to determine the structure-activity relationship and antagonistic mechanism on TRPM2 using whole-cell patch clamp and Ca^{2+} imaging in HEK293 cells with stable human TRPM2 expression. We show that tatM2NX inhibits over 90% of TRPM2 channel currents at concentrations as low as 2μM. Moreover, tatM2NX is a potent antagonist with an IC_{50} of 396nM. Our results from tatM2NX mutagenesis indicate that specific residues within the tatM2NX C-terminus are required to confer antagonism on TRPM2. Therefore, the peptide tatM2NX represents a new tool for the study of TRPM2 function in cell biology, also to enhance our understanding of TRPM2 in disease.

Significance statement

TatM2NX is a potent TRPM2 channel antagonist with the potential for clinical benefit in neurological diseases. This study characterizes interactions of tatM2NX with TRPM2 and the mechanism of action using structure-activity analysis.

Molecular Pharmacology Fast Forward. Published on November 26, 2019 as DOI: 10.1124/mol.119.117549
This article has not been copyedited and formatted. The final version may differ from this version.

Introduction

The Transient Receptor Potential Melastatin 2 (TRPM2) is a non-selective cation channel from the TRP family. At physiological membrane potentials, activation of TRPM2 results in influx of sodium and calcium into the cell. TRPM2 forms tetramers composed of six transmembrane domains with the N- and C-termini facing the intracellular milieu. The C-terminus contains a unique NUDT9-homology domain (NUDT9-H) required for adenosine diphosphate ribose (ADPR) binding and activation, absent in other TRP family members (Tong et al. 2006; Hantute-Ghesquier et al. 2018). TRPM2 was initially described as a channel/enzyme (chanzyme) due to the presence of the NUDT9-H domain. However, subsequent work has demonstrated that the C-terminal NUDT9-H domain of TRPM2 lacks enzymatic activity (Perraud et al. 2003; Iordanov et al. 2016). The NUDT9-H domain of TRPM2 is essential for intra- and interface interactions that regulate TRPM2 channel activation by ADPR (Wang et al. 2018; Huang et al. 2018). Intracellular calcium (Ca^{2+}) serves as a co-agonist, modulating channel activity in the presence of ADPR (Herson, Dulock, and Ashford 1997; Herson et al. 1999; Perraud et al. 2001; Inamura et al. 2003; McHugh et al. 2003; Kuhn and Luckhoff 2004; Heiner et al. 2006; Olah et al. 2009; Toth, Iordanov, and Csanady 2015; Yu et al. 2017; Fliegert, Watt, et al. 2017; Fliegert, Bauche, et al. 2017). Consistent with these physiological observations, the recently solved human TRPM2 channel structure indicates an ADPR binding site in the C-terminus that appears to interact with the N-terminus upon opening and leads to structural changes in a calcium-dependent ‘primed’ state (Huang et al. 2018; Wang et al. 2018).

TRPM2 channels have been implicated in several physiological and pathophysiological conditions in multiple organs (Verma et al. 2012; Shimizu et al. 2013; Gelderblom et al. 2014; Alim et al. 2013; Li and Jiang 2019; Park et al. 2016; Andoh et al. 2019; Haraguchi et al. 2012; Jang et al. 2015; Inamura et al. 2003; Smith et al. 2003; Fonfria et al. 2004; Kraft et al. 2004; Fonfria et al. 2006; Lange et al. 2009; Hoffman et al. 2015; Tan and McNaughton 2016). TRPM2

Molecular Pharmacology Fast Forward. Published on November 26, 2019 as DOI: 10.1124/mol.119.117549
This article has not been copyedited and formatted. The final version may differ from this version.

channels are highly expressed in the brain, found in neurons and microglia in the cortex, hippocampus, striatum, brainstem and others (Fonfria et al. 2006; Olah et al. 2009; Chung, Freestone, and Lipski 2011). TRPM2 channels are activated following oxidative stress, and the most well-characterized role for these channels is a cell death mediator following oxidative stress, due to excessive Ca^{2+} influx and consequent cell death (Fonfria et al. 2004; Perraud et al. 2005; Bai and Lipski 2010). However, the lack of specific TRPM2 channel antagonists has hindered the research regarding the role of TRPM2 channels in brain function, with most data coming from cell culture experiments or global TRPM2 channel genetic ablation in mice. Thus far, most described TRPM2 pharmacological inhibitors are not specific to TRPM2 channels, including antifungals, flufenamic acid, fenamate non-steroidal anti-inflammatories, 2-aminoethoxydiphenyl borate and natural compounds with moderate to high potency (Hill, McNulty, and Randall 2004; Chen et al. 2012; Starkus et al. 2017; Zhang et al. 2018). The TRPM2 inhibitor, JNJ-28583113, is a recently described inhibitor that appears promising, with nanomolar potency when applied to the extracellular surface of TRPM2 channels. However, is limited by stability difficulties in the brain (Fourgeaud et al. 2019). In contrast, we recently reported that the inhibitor, tatM2NX, reduces ischemic injury when administered following focal cerebral ischemia (Shimizu et al. 2016) and global cerebral ischemia (Dietz et al. 2019) *in vivo*, providing evidence for clinical benefit. Therefore, the aim of this study is to characterize the TRPM2 channel inhibitor tatM2NX, a peptide designed to interact with the ADPR binding site on the NUT9-H domain.

In this structure-activity relationship (SAR) study, we show that tatM2NX is an antagonist of human TRPM2 channels using whole-cell patch clamp and calcium imaging in HEK293 cells. Mutagenesis of tatM2NX reveals that the mechanism of action results from tatM2NX C-terminal interactions with TRPM2. Ultimately, tatM2NX is a potent pharmacological tool to disentangle TRPM2 function in cellular physiology and neurological diseases.

Materials and Methods

Protein Structure Prediction and Molecular Modeling: All molecular modeling studies were conducted using Biovia Discovery Studio 2018 (Biovia, Inc, Sand Diego, CA; www.3dsbiovia.com) and YASARA Structure 18.4 (YASARA Biosciences GmbH, Vienna, Austria; www.yasara.org). Structural coordinates for the human TRPM2 ion channel (Wang et al. 2018) were downloaded from the Protein Data Bank (www.rcsb.org, PDB accession: 6MIX). A*b initio* prediction of the secondary and tertiary structures for the wild-type, truncated, and mutant peptides was performed using the online QUARK server (https://zhanglab.ccmb.med.umich.edu/QUARK/) (Xu and Zhang 2012, 2013). The top 5 predicted peptide structures for each designed peptide were subjected to 1 nanosecond (ns) of explicit solvent-based molecular dynamic (MD) simulation utilizing the YASARA2 force field (Krieger et al. 2006; Krieger et al. 2009; Krieger et al. 2012; Krieger and Vriend 2015), which combines the AMBER (ff14SB) force field (Maier et al. 2015) with self-parameterizing knowledge-based potentials (Krieger, Koraimann, and Vriend 2002), to refine each of the predicted peptide structures. The snapshots from the resulting trajectories were assessed using the WHAT_IF and WHAT_CHECK (Hooft et al. 1996; Vriend 1990) structure validation tools to quantitatively evaluate the overall quality of each predicted structure, with the highest scoring structure for each peptide selected for further analysis. The ZDOCK (Chen, Li, and Weng 2003), ZRANK (Pierce and Weng 2007), and RDOCK (Li, Chen, and Weng 2003) algorithms were employed within Discovery Studio to predict the most likely protein-peptide complexes and refine their respective intermolecular interactions, as we have described previously (Ryan et al. 2012; Smith et al. 2018). To test the stability of the predicted interactions, we first removed the transmembrane domain of the TRPM2 subunit (residues 697-1165) and the top scoring complex for each peptide was placed in a simulation cell under periodic boundary conditions, filled with water, 0.9% NaCl and counter ions, pH7.4, at a temperature of 298K (Krieger et al. 2004). The main MD simulation was run for 5 ns using the AMBER (ff14SB) force field (Maier

Molecular Pharmacology Fast Forward. Published on November 26, 2019 as DOI: 10.1124/mol.119.117549
This article has not been copyedited and formatted. The final version may differ from this version.

et al. 2015) with GAFF (Wang et al. 2004) / AM1BCC (Jakalian, Jack, and Bayly 2002) parameters, particle mesh Ewald (PME) summation, an 8.0 Å cutoff for non-bonded forces, a 5 fs time-step, LINCS-constrained hydrogen atoms (Hess et al. 1997), and at constant pressure and temperature (the NPT ensemble), as described previously (Krieger and Vriend 2015). Figures were generated using Lightwave 2019 (NewTek Inc, Burbank, CA; www.lightwave3d.com) and Marmoset Toolbag 3.07 (Marmoset, LLC, Portland, OR; www.marmoset.co).

Cell Culture: Doxycycline-inducible N-terminal FLAG-TRPM2-expressing human embryonic kidney (HEK293) cells, provided by Anne L. Perraud (University of Colorado Anschutz Medical Campus, CO, USA), were cultured as previously described (Perraud et al. 2001; Shimizu et al. 2016). Briefly, cells were grown in Advanced DMEM medium containing 10% fetal bovine serum, 2mM Glutamatax (Life technologies, Carlsbad, CA, USA), and MycoZap-Plus (Lonza, Switzerland). Cell line authentication was confirmed as female human embryonic kidney cells and mycoplasma contamination was negative (BioResources Core, University of Colorado, Anschutz Medical Campus, Aurora, CO, USA). During growth, selection markers Zeocin (1µg/ml) (Invitrogen, Carlsbad, CA, USA) and Blastocidin-S (0.4µg/ml) (Gibco, Carlsbad, CA, USA) were utilized for the selective expression of Tet repressor and human TRPM2 in HEK293 cells until 80-90% confluence. Cells were grown for up to 20 passages (P3-P20). For Western blot experiments, HEK293-derived cells were maintained in Zeocin and Blastocidin-S (un-induced cells) or in doxycycline (1µg/mL) (induced cells) for 16-18h prior to protein lysate collection. For electrophysiology experiments, HEK293 cells were seeded on 12mm glass coverslips at a density of 12,000 cells/ml for 16-24h for doxycycline-inducible human TRPM2 expression prior to experiments. For Ca^{2+} imaging experiments, HEK293 cells were seeded on Mattek glass bottom dishes (Mattek Corporation, Ashland, MA, USA) at a density of 25,000 cells/ml for 16-24h prior to experiments.

Molecular Pharmacology Fast Forward. Published on November 26, 2019 as DOI: 10.1124/mol.119.117549
This article has not been copyedited and formatted. The final version may differ from this version.

Western blot: HEK293 cells were collected 16-18h after induction via centrifugation at 3,000rpm for 3min, washed in phosphate buffered saline (1xPBS, pH 7.4), and lysed for 10min using neuronal protein extraction reagent (Thermo Scientific, Rockford, IL, USA). For GSK3β expression and phosphorylation, HEK293 cells were pre-incubated with tatM2NX for 30min-4h followed by 250μM H_2O_2 stimulation (10min) and protein lysates collected immediately. Lysates were centrifuged at 12,000rpm for 15min and supernatant collected for protein quantification. Protein samples (15-20μg) were resolved using SDS-PAGE, and transferred in PVDF membranes (β-actin, 50min; FLAG-TRPM2, 90min; GSK3β, 50min). PVDF membranes were blocked in 5% bovine serum albumin for 1h and incubated overnight at 4°C in primary antibody. Human TRPM2 expression was assessed with mouse anti-FLAG (1:1000, F1804, Sigma, St. Louis MO, USA) (Brizzard, Chubet, and Vizard 1994), and normalized to mouse anti-β-actin peroxidase (1:10000, A3854, Sigma, St. Louis, MO, USA). GSK3β phosphorylation and expression was assessed with rabbit anti-pGSK3 or GSK3β (1:1000, 9323S; and 1:1000, 12456S, Cell Signaling Technology, Danvers, MA, USA). All membranes were washed 3 times, incubated in secondary horseradish peroxidase-conjugated goat-anti mouse or goat-anti rabbit antibody (1:10000, 115-035-174 or 115-035-003, ImmunoResearch Laboratories, USA; or 1:10000, 31460, ThermoFisher Scientific, USA) for 1h at room temperature. Western blot bands were detected using the SuperSignal™ West Femto Maximum Sensitivity Substrate (34096, ThermoFisher Scientific, USA) and imaged with BioRad ChemiDoc MP Imaging System (Hercules, CA, USA).

Immunocytochemistry: Doxycycline-inducible human TRPM2-expressing HEK293 cells (16-18h) were fixed with 4% paraformaldehyde for 10min on ice, washed in 1xPBS, permeabilized using 0.3% TritonX-100 dissolved in 1xPBS for 10min at room temperature, and blocked in 4% bovine serum albumin overnight at 4°C. For biotin-tatM2NX detection, HEK293 cells were incubated with the peptide for 1h prior to fixation. Primary antibody (mouse-anti-FLAG, 1:1000,

Molecular Pharmacology Fast Forward. Published on November 26, 2019 as DOI: 10.1124/mol.119.117549
This article has not been copyedited and formatted. The final version may differ from this version.

F1804, Sigma, St. Louis MO, USA) was incubated for 2h at room temperature in 2.5% BSA/PBS and secondary antibody (594-conjugated streptavidin, 1:1000, 016-540-084; or 488-donkey-anti-mouse, 1:1000, 715-545-150; ImmunoResearch Laboratories, West Grove, PA, USA) for 1h at room temperature in 2.5% BSA/PBS. Then, coverslips were mounted using Prolong Gold Antifade Agent (Thermo Fisher Scientific, USA). Images of HEK293 cells were taken at room temperature on an Olympus IX83 (Olympus Fluoview FV1200 Laser Scanning Confocal Microscope; Olympus Life Science, MA, USA) using a 20x objective. Two individual observers analyzed all images.

Co-immunoprecipitation: Protein lysates (500µg) from doxycycline-inducible human TRPM2-expressing HEK293 cells (16-18h) containing a N-terminal FLAG tag were incubated for 1h with N-terminal biotin-tagged tatM2NX (20µg) following addition of prewashed streptavidin-conjugated agarose (60µl, 16-126, Sigma Aldrich, St. Louis, MO, USA) at 4°C on a rocker. Samples were washed three times with phosphate buffer (100mM NaCl, pH 7.4). Purified biotin-tatM2NX complexes with FLAG-TRPM2 were boiled at 95°C for 5min in Laemmli dye (40-50µl, BioRad, USA). Bands were resolved using Precast Miniprotean gradient gels (4-20% acrylamide, BioRad, USA) cut in half and transferred 30min for biotin-tatM2NX (5kDa) and 90min for FLAG-TRPM2 (170kDa) in PVDF membranes (0.22 or 45µm). FLAG-TRPM2 was probed using primary mouse anti-FLAG M2 antibody (F1804, Sigma Aldrich, USA), and secondary horseradish peroxidase-conjugated goat anti-mouse (1:10000, 115-035-003 or 111-035-003 ImmunoResearch Laboratories, USA). See Western blot for membrane development.

Peptide synthesis: TatM2NX and derivatives were synthetized commercially with >95% purity (Chi Scientific, Maynard, MA, USA). All peptides contained a cell-permeant N-terminus tat-HIV sequence (YGRKKRRQRRR) fused to the M2NX sequence variations (Table 1). For co-immunoprecipitation, biotin was conjugated to tatM2NX.

Electrophysiology: All recordings were performed in HEK293 cells and currents amplified with Axopatch 200B (Axon Instruments, USA), digitized with DigiData1550B, and controlled using

Molecular Pharmacology Fast Forward. Published on November 26, 2019 as DOI: 10.1124/mol.119.117549
This article has not been copyedited and formatted. The final version may differ from this version.

pClamp10.7 software (Molecular Devices, CA, USA). Signals were filtered at 5kHz and digitized at 1kHz. Glass borosilicate electrodes (3.5-5MΩ) were used to record human TRPM2 currents activated by +40mV voltage-step from 0mV in whole-cell voltage clamp configuration. The protocol was chosen to produce an outward current and therefore reduce TRPM2-mediated calcium influx and subsequent cell death. All experiments were performed with HEPES-buffered saline containing in mM: 140 NaCl, 2.5 KCl, 10 HEPES, 5 glucose, 1 $MgCl_2$, 1 CaCl, pH 7.4. The internal solution contained in mM: 145 K-gluconate, 0.05 EGTA (for physiological buffering of Ca^{2+} at 100-200nM), 1 $MgCl_2$, 10 HEPES, pH 7.3. For antagonism, the internal solution contained 100µM ADPR (A0752, Sigma Aldrich, St. Louis, MO, USA) and 0, 0.05, 0.15, 0.3, 0.5, 2, 5 or 10µM tatM2NX. The inclusion of tatM2NX in the internal solution allows access of controlled concentration to the intracellular ADPR binding site on TRPM2, however no solution exchange is possible to assess reversibility. For competitive antagonism, the internal solution contained 500µM ADPR and 0 or 2µM tatM2NX. For structure-activity relationship (SAR) experiments, the internal solution contained 100µM ADPR and 2µM peptide (tatWV-AA, tat Cterm, tat Nterm). We added clotrimazole (CTZ, 20µM, C6019-G, Sigma, St. Louis, MO, USA) after steady-state inhibition as a positive control. Exclusion criteria was based on access resistance R_a<15MΩ and remaining leak current <350pA after CTZ inhibition.

Ca^{2+} Imaging: Live cell imaging of HEK293 cells was performed at room temperature on an Olympus IX83 (Olympus Fluoview FV1200 Laser Scanning Confocal Microscope; Olympus Life Science, MA, USA) using a 10x objective. For all imaging experiments in this study, controls and peptides were tested each experimental day to account for passage differences. All images were processed using FIJI Software (Rueden et al. 2017). Each plate was washed 3 times with HEPES-buffered saline (see electrophysiology above). A total volume of 2ml was added to each plate with 5µM of the Ca^{2+} indicator Fluo5F, AM (Invitrogen, Eugene, OR, USA), with or without 2µM peptide (tatWV-AA, tat Cterm, tat Nterm), or 20µM CTZ and incubated at 37°C for 40-50min prior to

Molecular Pharmacology Fast Forward. Published on November 26, 2019 as DOI: 10.1124/mol.119.117549
This article has not been copyedited and formatted. The final version may differ from this version.

experiments. Then, plates were washed and fresh solution added with or without drugs. Excitation illumination was delivered every 10sec for 20min. After 1min baseline, TRPM2 activity was stimulated using 250μM H_2O_2 and fluorescence recorded for 20min. Cells were incubated with antagonist prior to exposure to H_2O_2, which activates TRPM2 channels, resulting in cell death within 30-60min as uncontrolled Ca^{2+} influx through activated TRPM2 channels is toxic to cells. Therefore, we chose to image for 20min to assess the inhibition of each peptide, and unable to assess reversibility.

Statistical Analysis: For analysis of steady-state inhibition of TRPM2 currents, a paired or independent samples *t*-test was performed with statistical significance of $p<0.05$ for n≥4-10. Potency (IC_{50}) was determined using a non-linear regression analysis (Log of inhibitor concentration versus normalized response) equation: Y=100/(1+10^((X-LogIC50))); x= log of concentration, y=normalized response (current density pA/pF), using Graph Pad Prism version 8.0.2 for Windows, GraphPad Software, La Jolla California USA, www.graphpad.com**.** For Ca^{2+} imaging, changes in F/F_0 (n=6-12 individual cells/plate) was used to compare groups after normalizing to background fluorescence. Individual ROI were drawn for each cell and analyzed using Time Series Analyzer plugin in FIJI Software (Rueden et al. 2017). Area under the curve for each group was determined and groups were compared to control H_2O_2 using One-Way ANOVA with Dunnett's post-hoc test for multiple group comparison. Statistical significance was determined as $p<0.05$ and all groups represented as mean±SD.

Results

Modeling for tatM2NX antagonism on TRPM2

We recently showed the peptide tatM2NX is a TRPM2 antagonist with selective neuroprotective effects in a mouse model of focal ischemia (stroke) (Shimizu et al. 2016) and global ischemia (CA/CPR) (Dietz et al. 2019). To characterize the mechanism of TRPM2 inhibition by tatM2NX, we performed molecular modeling (MD) to allow prediction of tatM2NX

Molecular Pharmacology Fast Forward. Published on November 26, 2019 as DOI: 10.1124/mol.119.117549
This article has not been copyedited and formatted. The final version may differ from this version.

interaction/inhibition of activity and potential key residues responsible for efficacy. *Ab initio* prediction of the secondary and tertiary structure of the parent tatM2NX peptide was predicted to adopt a single, alpha helical structure that remained stable during MD-based refinement and analysis (**Figure 1A, Table 1**).

Protein-peptide complex prediction for tatM2NX indicated that the top scoring cluster for the peptide involved direct interaction with the human ADPR binding site (**Figure 1B**), which suggests occlusion of this site and the resulting inhibition of ADPR binding as a potential mechanism for the observed functional inhibition of TRPM2 *in vitro*. To test the stability of the predicted complex, we performed a 5ns MD-based simulation in the presence of an explicit solvent. The TRPM2-tatM2NX complex remained stable throughout the simulation and appeared to settle further into the ADPR binding site and enhance the number of favorable interactions between tatM2NX and TRPM2 compared to the initial predicted complexes (**Figure 1C, Table 2**). At the end of the MD simulation period, tatM2NX made several favorable intermolecular interactions, including salt-bridges with Arg1280 and Arg1433 as well as an extensive network of intermolecular hydrogen bonds and hydrophobic interactions (**Table 2**). TatM2NX also appeared to form a wedge-like conformation, with the C-terminus portion interacting with the ADPR binding site and the Tat-HIV tag (N-terminus) interacting with the opposite side the TRPM2 monomer (**Figure 1C, right**).

Human TRPM2 channels are expressed and functional in HEK293 cells

We measured TRPM2 protein expression and function in HEK293 cells. Human TRPM2 (N-terminal FLAG tag) is expressed in HEK293 cells after doxycycline treatment (16-18h) **(Supplemental Figure 1A, B).** To validate human TRPM2 channel function, we performed whole cell patch-clamp experiments in HEK293 cells with ADPR present in the pipette solution to stimulate TPRM2-mediated currents. We found that human TRPM2 exhibited large initial current density ($ADPR_i$, 184.4 ± 63.73 pA/pF, n=5) exclusively under doxycycline treatment

Molecular Pharmacology Fast Forward. Published on November 26, 2019 as DOI: 10.1124/mol.119.117549
This article has not been copyedited and formatted. The final version may differ from this version.

(**Supplemental Figure 1C, Figure 2A**). We observed significant rundown of TRPM2 initial current density ($ADPR_f$, 86.45 ± 46.68 pA/pF, n=5; *p*<0.05), which reached steady-state levels after 2-3min, as previously described (Toth and Csanady 2012) **(Supplemental Figure 1C).** Therefore, subsequent experimental analysis was performed using the steady state current density at 3min as the active TRPM2 current ($ADPR_f$). Multiple control experiments were performed to confirm the ADPR-induced current in HEK293 cells were carried by TRPM2 channels. Importantly, the TRPM2 channel pore-blocker Clotrimazole (20μM CTZ) abolished ADPR currents (6.359 ± 3.666 pA/pF, n=5; p<0.05) (**Supplemental Figure 1C**). Also, un-induced (no-doxycycline treatment) cells lacked TRPM2 expression or activity (0.58 ± 0.765 pA/pF vs 0.09± 1.67 pA/pF, p>0.05) (**Supplemental Figure 1A, 1D**). These results validate TRPM2 expression and function in doxycycline-treated HEK293 cells.

TatM2NX is a potent TRPM2 antagonist

To characterize tatM2NX as an antagonist we performed a dose-response study. To achieve a known concentration of ligand and antagonist within each HEK293 cell, we used whole-cell patch clamp with 100μM ADPR and tatM2NX added to the internal solution (pipette) allowing them to freely dialyze into the cell once whole cell access was obtained. Our results show a concentration-dependent decrease in TRPM2 current density. We observed approximately 75% inhibition of initial TRPM2 current at 0.5μM tatM2NX (37.82 ± 53.19 pA/pF, n=5; p<0.05), and approximately 90% inhibition at 2μM (10.27 ± 9.52 pA/pF, n=7; p<0.05), 5μM (7.76 ± 6.387 pA/pF, n=5; *p*<0.05), and 10μM tatM2NX (13.17 ± 13.36, n=4; p<0.05) (**Figure 2A, B**). This inhibition was reached within 6-8min. No significant differences were observed for 0.15μM (121.6 ± 62.65 pA/pF, p>0.05), 0.3μM (118.0 ± 50.68 pA/pF, p>0.05) tatM2NX compared to 0.05 μM (142.2 ± 90.81 pA/pF, n=7) (**Figure 2B**), which was similar to ADPR alone ($ADPR_f$, 86.45 ± 46.68 pA/pF, n=5, p>0.05) (**Supplemental Figure 1E**). A non-linear regression method (log inhibitor concentration versus normalized response) of the tatM2NX dose-response estimated a potency

Molecular Pharmacology Fast Forward. Published on November 26, 2019 as DOI: 10.1124/mol.119.117549
This article has not been copyedited and formatted. The final version may differ from this version.

(IC_{50}) of 3.96e-007 ± 0.05868 (396nM) (**Figure 2C**). These results suggest that tatM2NX is a potent antagonist of TRPM2 currents in the presence of ADPR.

To validate tatM2NX binding to TRPM2 as predicted in our molecular modeling, we performed co-immunoprecipitation using the N-terminal biotin-tag on tatM2NX. To do this, we extracted whole-cell protein lysates from HEK293 cells and incubated protein lysates (500µg) with biotinylated-tatM2NX (20µg). The peptide biotin-tatM2NX formed a complex with FLAG-TRPM2 when co-immunoprecipitated using streptavidin-conjugated agarose (**Figure 3A**). This binding interaction is specific to HEK293 cells expressing TRPM2 (lane 3) and absent in un-induced cells (lane 4) or beads without biotin-tatM2NX (lane 1). These results indicate that tatM2NX directly interacts with TRPM2.

We next assessed the ability of tatM2NX to inhibit TRPM2-mediated dephosphorylation of GSK-3β (activation), as this signaling pathway has recently been shown in cell culture (Fourgeaud et al. 2019) and brain slices (Dietz et al. 2019). TRPM2 stimulation with H_2O_2 (250µM) activates GSK3β (dephosphorylation) in HEK293 cells (+control) compared to untreated cells (-control) (**Figure 3B**). Pre-incubation with tatM2NX (2µM) for 2-4h prevents GSK3β activation indicating that tatM2NX inhibits TRPM2-mediated GSK3β signaling (**Figure 3B**).

To determine whether tatM2NX acts as a competitive antagonist for human TRPM2 channels, we tested the antagonistic capacity of 2µM tatM2NX in the presence of 500µM ADPR. In these ligand saturating conditions, $ADPR_i$ were similar in control (173.1 ± 45.22 pA/pF, n=4) and in the presence of 2µM tatM2NX (193.4 ± 78.00 pA/pF, n=4) (**Figure 3C**). Interestingly, 2µM tatM2NX failed to inhibit $ADPR_f$ current density (89.22 ± 42.22 pA/pF, n=4; $p>0.05$) compared to control (117.0 ± 10.53, n=4) indicating that higher concentrations of ADPR can prevent tatM2NX antagonism (**Figure 3C**). These results indicate that tatM2NX is a competitive antagonist of TRPM2 and serves to validate the results of our molecular modeling simulations.

TatM2NX C-terminus is sufficient to antagonize TRPM2 in cells

Molecular Pharmacology Fast Forward. Published on November 26, 2019 as DOI: 10.1124/mol.119.117549
This article has not been copyedited and formatted. The final version may differ from this version.

Based on the initial molecular modeling of tatM2NX in complex with TRPM2, we identified two bulky hydrophobic residues, tryptophan in position 33 and valine in position 34 (W33, V34) within the C-terminus that remained buried within the ADPR binding site throughout the molecular modeling simulation. We hypothesized that mutating these two residues would potentially abrogate the binding of tatM2NX to the ADPR binding site. Molecular modeling of tatM2NX with W33A and V34A mutations to W33V34 (tat-WVAA) indicated a loss of interaction with the ADPR binding site in any of the top 3 scoring interaction clusters (**Supplemental Figure 2A**) nor did we observe any substantive interactions with this site in any of the lower scoring results (data not shown). We performed additional computational simulations to assess the capacity of a truncated form of tatM2NX (tat Cterm; containing the last 23 amino acids) to preserve these interactions with the ADPR binding site. The peptide tat Cterm interacts with the ADPR binding site similarly to the parent peptide tatM2NX (**Supplemental Figure 2A, 2C**). This suggested that the C-terminus of tatM2NX was sufficient to interact with the ADPR binding site and would likely recapitulate the inhibitory effects of the parent peptide tatM2NX on TRPM2. Similar to tatM2NX, the tat Cterm peptide was predicted to maintain and enhance interactions with the ADPR binding site over the simulation period (**Supplemental Figure 2B, 2C, Supplemental Table 1**). In contrast, the interactions of the tatWV-AA peptide did not appear stable and had substantial dissociation from TRPM2 (**Supplemental Figure 2B, 2D**) suggesting that tatWV-AA lacks physiologically relevant interactions with TRPM2. The overall structure of both tat Cterm and tatWV-AA peptides were highly similar in terms of secondary/tertiary structure (**Supplemental Figure 2B**).

Our molecular modeling predicted that stable interactions of tat Cterm and that mutating W33V34 to AA would result in a loss of interaction with the ADPR binding site. To validate the molecular modeling results, we performed electrophysiology and cell-based functional assays using Ca^{2+} imaging. In whole-cell patch clamp, the peptide tat-WVAA contained within the C-

Molecular Pharmacology Fast Forward. Published on November 26, 2019 as DOI: 10.1124/mol.119.117549
This article has not been copyedited and formatted. The final version may differ from this version.

terminus (**Table 1**) lacks antagonism on TRPM2 (116.3 ± 66.90 pA/pF, n=6; p>0.05) compared to $ADPR_f$ (89.39 ± 32.38 pA/pF, n=5), indicating that either/both residues are required to confer antagonism (**Figure 4A**). Because the tat Cterm peptide clustered by the ADPR binding site, we tested N- and C-termini truncated peptides (23 amino acids each) to determine the extent of antagonism by these truncated forms of tatM2NX (Table 1)**.** In whole-cell patch clamp experiments, tat Cterm displayed significant antagonism (15.56 ± 7.52 pA/pF, n=6; *p*<0.05) compared to $ADPR_f$ **(Figure 4A).** The N-terminus truncation (tat Nterm) did not inhibit TRPM2 (141.2 ± 31.47 pA/pF, n=4; p<0.05) compared to $ADPR_f$ (**Figure 4A**). These results suggest that tatM2NX C-terminus is sufficient to inhibit TRPM2 while the N-terminus alone lacks antagonistic effect. Also, these confirms that the tat-HIV tag, and not the N-terminus sequence, is responsible for direct interactions with TRPM2 and requires the C-terminus residues W33V34 in proximity to the ADPR binding site. Lastly, all $ADPR_i$ currents were similar in the presence of peptides compared to control (**Supplemental Figure 3A)**.

To verify that tatM2NX was cell permeable, we incubated biotin-tatM2NX with HEK293 cells for 1h, followed by immunocytochemistry for N-terminal tagged biotin-tatM2NX and N-terminal tagged FLAG-TRPM2 within HEK293 cells (**Supplemental Figure 1B**). To test whether these peptides show antagonistic effects when applied extracellularly, we measured Ca^{2+} in HEK293 cells in response to H_2O_2 stimulation. H_2O_2 stimulated Ca^{2+} influx through TRPM2 in control group (77,441 ± 34,790 F/F_0 x min; n=53) as previously described (Herson et al. 1999; Shimizu et al. 2016; Kraft et al. 2004; Olah et al. 2009) (**Figure 4B, 4C**). TatM2NX, tat Cterm and CTZ significantly decreased Ca^{2+} fluorescence (F/F_0) after 20min (47,904 ± 31,245 F/F_0 x min; n=48, p<0.05; 50,600 ± 26,993 F/F_0 x min; n=49, p<0.05; 31,910 ± 10,880 F/F_0 x min; n=25, p<0.05, respectively) (**Figure 4B, 4C, 4D**). However, tat Nterm (67,851 ± 33,830 F/F_0 x min; n=48, p>0.05) had no effect on Ca^{2+} fluorescence activated by H_2O_2 (**Figure 4C, 4D**). On the other hand, Ca^{2+} fluorescence with tat-WVAA is higher than H_2O_2 (99,192 ± 39,653 F/F_0 x min; n=52, p<0.05)

Molecular Pharmacology Fast Forward. Published on November 26, 2019 as DOI: 10.1124/mol.119.117549
This article has not been copyedited and formatted. The final version may differ from this version.

(**Figure 4D**). All cellular responses in the presence of peptides had similar fluorescent kinetics as H_2O_2 stimulation alone (H_2O_2, 105.27 ± 16.81 frames; tatM2NX, 106.48 ± 18.73 frames; tat Cterm, 107 ± 19.06 frames; tat Nterm, 110.19 ± 14.07 frames; tat-WVAA, 102.81 ± 22.10 frames) (**Supplemental Figure 3B**). These data suggest that tat Cterm inhibits TRPM2 activity in cells at similar levels as tatM2NX and residues W33V34 are essential for antagonism.

Discussion

In this study, we evaluated the pharmacological properties of tatM2NX on TRPM2 channels and found evidence of potent inhibition; with an IC_{50} of approximately 396nM. Furthermore, we identified two residues within tatM2NX C-terminus, W33 and V34, necessary for antagonism. Our molecular modeling of TRPM2 (in the closed channel state) and tatM2NX show direct interactions of tatM2NX with the ADPR binding site. These results are consistent with co-immunoprecipitation of tatM2NX and reduce inhibition in the presence of excess ADPR. Recently, cryoEM structures validated previous TRPM2 mutagenesis studies indicating that the ADPR binding site is contained within NUDT9-H (Huang et al. 2018; Kuhn and Luckhoff 2004; Shen et al. 2003; Wang et al. 2018; Yu et al. 2017). TRPM2 undergoes conformational changes in the C-terminus NUDT9-H domain priming an open-channel state upon ADPR binding. Our results support that tatM2NX disrupts the ability of ADPR to open TRPM2 channels. This is the first characterization, to our knowledge, of a peptide inhibitor targeting TRPM2 with *in vivo* applications.

The tatM2NX peptide was predicted to both directly interact, through its C-terminus, with the human ADPR binding site and to remain wedged in place via the interactions of the tat-HIV (permeability sequence) outside of the ADPR site. Activation of TRPM2 involves extensive conformational changes to the cytosolic N- and C-terminal regions of TRPM2 that bring the globular domains in closer proximity to one another (Huang et al. 2018; Wang et al. 2018). The modeling results suggest that, in addition to occluding the ADPR binding site, tatM2NX may also

Molecular Pharmacology Fast Forward. Published on November 26, 2019 as DOI: 10.1124/mol.119.117549
This article has not been copyedited and formatted. The final version may differ from this version.

directly impede the molecular mechanics of activation by blocking or impairing these conformational changes.

The interactions of tat Cterm with the ADPR binding site were stable and the peptide itself moved further into the ADPR binding site over the simulation period. These results suggest that the C-terminus hydrophobic interactions with the ADPR binding site are sufficient to maintain the TRPM2-tat Cterm interactions. Interestingly, the best predicted complexes for the active inhibitory peptides involved binding at the human ADPR site with extensive stable interactions (**Supplemental Table 1**). Future mutagenesis studies may reveal which interactions are required for inhibition. Other top ranked complexes for both tatM2NX and tat Cterm peptides involved interaction with the region corresponding to the ADPR binding site in zebrafish TRPM2 (Huang et al. 2018; Fliegert, Holzer, and Guse 2018) suggesting that these peptides may also have inhibitory effects against the activity of zebrafish TRPM2. Also, we have shown efficacy in mouse models of brain ischemia (Shimizu et al. 2016; Dietz et al. 2019), therefore this tool has potential use in multiple systems and species.

Isolating TRPM2 function in physiology and pathophysiology is critical to understand signaling downstream of TRPM2 channel activation. Previous studies used non-specific pharmacological inhibitors to show the involvement of TRPM2 function increasing oxidative stress signaling (Fonfria et al. 2004; Perraud et al. 2005). More recently, total genetic ablation approaches in rodents associate TRPM2 with mood disorders, social interactions, temperature control, and Alzheimer's disease implicating increased TRPM2 channel activity to various neurological diseases across many brain regions (Andoh et al. 2019; Jang et al. 2015; Alawieyah Syed Mortadza et al. 2018; Ostapchenko et al. 2015; Tan and McNaughton 2016). Therefore, pharmacological targeting of this channel has the potential to provide clinical benefit in several neurological disorders. However, there are not available inhibitors that would be amenable to clinical use. We believe tatM2NX represents the most promising TRPM2 pharmacological inhibitor

Molecular Pharmacology Fast Forward. Published on November 26, 2019 as DOI: 10.1124/mol.119.117549
This article has not been copyedited and formatted. The final version may differ from this version.

available to date. A single dose of tatM2NX effectively crosses the blood-brain barrier while providing TRPM2 specific neuroprotection in stroke and cardiac arrest animals, setting precedence for the use of tatM2NX *in vivo* (Shimizu et al. 2016; Dietz et al. 2019). These studies demonstrate the ability of tatM2NX to cross the BBB and impact brain injury, consistent with several previous studies showing tat-conjugated proteins crossing the BBB (Rizzuti et al. 2015; Lalatsa, Schatzlein, and Uchegbu 2014; Cao et al. 2002; Hill et al. 2012). Further, our recent study in cardiac arrest implicated TRPM2 channel inhibition of GSK-3β in long-term functional deficits (Dietz et al. 2019). Consistent with this, data presented here shows that tatM2NX prevents oxidative stress-induced activation (dephosphorylation) of GSK-3β. In *ex vivo* experiments with the human TRPM2 channel, tatM2NX inhibits with similar high potency as JNJ-28583113 (Fourgeaud et al. 2019) and scalaradial, another potent TRPM2 antagonist that also targets TRPM7 (Starkus et al. 2017). Further, we assessed specificity of tatM2NX for TRPM2 (Shimizu et al. 2016) by showing no additional efficacy in TRPM2-/- mice on neuroprotection following stroke. Additionally, TRPM2 expression in other organs magnifies the use of tatM2NX in a variety of disease models (Park et al. 2016; Lange et al. 2009; Almasi et al. 2018). Future studies will determine the reversibility and specificity of tatM2NX. Further, comparison of TRPM channels 4, 7, and 8 binding pockets indicates that the ADPR binding site on TRPM2 is different (Supplemental Figure 4). Future studies will address off-target effects and confirm the molecular modeling performed for TRPM channel members and other proteins.

TatM2NX is a cell-permeable inhibitor with high potency, which makes extensive non-covalent interactions and favorable contacts with a number of residues of the ADPR binding site within the NUDT9-H domain. Many of these interactions were predicted and maintained in the tat Cterm peptide. In contrast, there were no predicted interactions between tatWV-AA and the ADPR binding site. Furthermore, both tatM2NX and tat Cterm exhibited competitive inhibition in cells, providing validation of the *in silico* predictions. Taken together, these data provide a mechanistic

rationale for the observed inhibition of TRPM2 channels. Due to the technical constraints of our experiments (see methods section), we were not able to assess the kinetics of inhibition or possible reversibility of tatM2NX. Our data indicates that tatM2NX is a competitive antagonist, leading us to speculate that tatM2NX is likely a reversible inhibitor binding at the ADPR binding site. Further experiments are needed to determine the reversal kinetics of this cell-permeable TRPM2 channel antagonist. Nonetheless, our *in vivo* data (Shimizu et al. 2016; Dietz et al. 2019) shows effective inhibition of TRPM2 channels in the intact brain, making this a valuable research tool for the study of TRPM2 channels. Beyond the characterization of tatM2NX as a novel TRPM2 antagonist, our aim is to provide a research tool that will move the field of TRP channels forward and aid in specifically studying TRPM2 molecular mechanisms in cell physiology and pathophysiology of diseases. The peptide tatM2NX will serve as a potential source of a new generation of derivatives that may be more potent and specific at antagonizing TRPM2.

Acknowledgements

We thank Dr. Anne Perraud for providing HEK293 cells containing a N-terminal FLAG epitope tag in a modified pCDNA4/TO vector. Special thanks to the Computational Chemistry and Biology Core Facility at the University of Colorado Anschutz Medical Campus for assistance with the structural modeling and simulation studies. This research was supported by National Institutes of Health grants T32GM007635 (Pharmacology training grant), R01NS092645 (to P.S.H).

Author Contributions

Participated in research design: I.C.T., D.S.B., P.S.H

Conducted experiments: I.C.T., D.S.B.

Contributed new reagents or analytic tools: I.C.T., D.S.B., P.S.H

Performed data analysis: I.C.T., D.S.B., P.S.H

Wrote or contributed to the writing of the manuscript: I.C.T., D.S.B., P.S.H

References

Alawieyah Syed Mortadza, S., J. A. Sim, V. E. Neubrand, and L. H. Jiang. 2018. 'A critical role of TRPM2 channel in Abeta42 -induced microglial activation and generation of tumor necrosis factor-alpha', *Glia*, 66: 562-75.

Alim, I., L. Teves, R. Li, Y. Mori, and M. Tymianski. 2013. 'Modulation of NMDAR subunit expression by TRPM2 channels regulates neuronal vulnerability to ischemic cell death', *J Neurosci*, 33: 17264-77.

Almasi, S., B. E. Kennedy, M. El-Aghil, A. M. Sterea, S. Gujar, S. Partida-Sanchez, and Y. El Hiani. 2018. 'TRPM2 channel-mediated regulation of autophagy maintains mitochondrial function and promotes gastric cancer cell survival via the JNK-signaling pathway', *J Biol Chem*, 293: 3637-50.

Andoh, C., N. Nishitani, E. Hashimoto, Y. Nagai, K. Takao, T. Miyakawa, T. Nakagawa, Y. Mori, K. Nagayasu, H. Shirakawa, and S. Kaneko. 2019. 'TRPM2 confers susceptibility to social stress but is essential for behavioral flexibility', *Brain Res*, 1704: 68-77.

Bai, J. Z., and J. Lipski. 2010. 'Differential expression of TRPM2 and TRPV4 channels and their potential role in oxidative stress-induced cell death in organotypic hippocampal culture', *Neurotoxicology*, 31: 204-14.

Brizzard, B. L., R. G. Chubet, and D. L. Vizard. 1994. 'Immunoaffinity purification of FLAG epitope-tagged bacterial alkaline phosphatase using a novel monoclonal antibody and peptide elution', *Biotechniques*, 16: 730-5.

Cao, G., W. Pei, H. Ge, Q. Liang, Y. Luo, F. R. Sharp, A. Lu, R. Ran, S. H. Graham, and J. Chen. 2002. 'In Vivo Delivery of a Bcl-xL Fusion Protein Containing the TAT Protein Transduction Domain Protects against Ischemic Brain Injury and Neuronal Apoptosis', *J Neurosci*, 22: 5423-31.

Chen, G. L., B. Zeng, S. Eastmond, S. E. Elsenussi, A. N. Boa, and S. Z. Xu. 2012. 'Pharmacological comparison of novel synthetic fenamate analogues with econazole and 2-APB on the inhibition of TRPM2 channels', *Br J Pharmacol*, 167: 1232-43.

Chen, R., L. Li, and Z. Weng. 2003. 'ZDOCK: an initial-stage protein-docking algorithm', *Proteins*, 52: 80-7.

Chung, K. K., P. S. Freestone, and J. Lipski. 2011. 'Expression and functional properties of TRPM2 channels in dopaminergic neurons of the substantia nigra of the rat', *J Neurophysiol*, 106: 2865-75.

Dietz, R. M., I. Cruz-Torres, J. E. Orfila, O. P. Patsos, K. Shimizu, N. Chalmers, G. Deng, E. Tiemeier, N. Quillinan, and P. S. Herson. 2019. 'Reversal of Global Ischemia-Induced Cognitive Dysfunction by Delayed Inhibition of TRPM2 Ion Channels', *Transl Stroke Res*.

Fliegert, R., A. Bauche, A. M. Wolf Perez, J. M. Watt, M. D. Rozewitz, R. Winzer, M. Janus, F. Gu, A. Rosche, A. Harneit, M. Flato, C. Moreau, T. Kirchberger, V. Wolters, B. V. L. Potter, and A. H. Guse. 2017. '2'-Deoxyadenosine 5'-diphosphoribose is an endogenous TRPM2 superagonist', *Nat Chem Biol*, 13: 1036-44.

Fliegert, R., H. T. Holzer, and A. H. Guse. 2018. 'TRPM2 activation: Paradigm shifted?', *Cell Calcium*, 76: 132-34.

Fliegert, R., J. M. Watt, A. Schobel, M. D. Rozewitz, C. Moreau, T. Kirchberger, M. P. Thomas, W. Sick, A. C. Araujo, A. Harneit, B. V. L. Potter, and A. H. Guse. 2017. 'Ligand-induced activation of human TRPM2 requires the terminal ribose of ADPR and involves Arg1433 and Tyr1349', *Biochem J*, 474: 2159-75.

Fonfria, E., I. C. Marshall, C. D. Benham, I. Boyfield, J. D. Brown, K. Hill, J. P. Hughes, S. D. Skaper, and S. McNulty. 2004. 'TRPM2 channel opening in response to oxidative stress is dependent on activation of poly(ADP-ribose) polymerase', *Br J Pharmacol*, 143: 186-92.

Fonfria, E., P. R. Murdock, F. S. Cusdin, C. D. Benham, R. E. Kelsell, and S. McNulty. 2006. 'Tissue distribution profiles of the human TRPM cation channel family', *J Recept Signal Transduct Res*, 26: 159-78.

Fourgeaud, L., C. Dvorak, M. Faouzi, J. Starkus, S. Sahdeo, Q. Wang, B. Lord, H. Coate, N. Taylor, Y. He, N. Qin, A. Wickenden, N. Carruthers, T. W. Lovenberg, R. Penner, and A. Bhattacharya. 2019. 'Pharmacology of JNJ-28583113: A novel TRPM2 antagonist', *Eur J Pharmacol*.

Gelderblom, M., N. Melzer, B. Schattling, E. Gob, G. Hicking, P. Arunachalam, S. Bittner, F. Ufer, A. M. Herrmann, C. Bernreuther, M. Glatzel, C. Gerloff, C. Kleinschnitz, S. G. Meuth, M. A. Friese, and T. Magnus. 2014. 'Transient receptor potential melastatin subfamily member 2 cation channel regulates detrimental immune cell invasion in ischemic stroke', *Stroke*, 45: 3395-402.

Hantute-Ghesquier, A., A. Haustrate, N. Prevarskaya, and V. Lehen'kyi. 2018. 'TRPM Family Channels in Cancer', *Pharmaceuticals (Basel)*, 11.

Haraguchi, K., A. Kawamoto, K. Isami, S. Maeda, A. Kusano, K. Asakura, H. Shirakawa, Y. Mori, T. Nakagawa, and S. Kaneko. 2012. 'TRPM2 contributes to inflammatory and neuropathic pain through the aggravation of pronociceptive inflammatory responses in mice', *J Neurosci*, 32: 3931-41.

Heiner, I., J. Eisfeld, M. Warnstedt, N. Radukina, E. Jungling, and A. Luckhoff. 2006. 'Endogenous ADP-ribose enables calcium-regulated cation currents through TRPM2 channels in neutrophil granulocytes', *Biochem J*, 398: 225-32.

Herson, P. S., K. A. Dulock, and M. L. Ashford. 1997. 'Characterization of a nicotinamide-adenine dinucleotide-dependent cation channel in the CRI-G1 rat insulinoma cell line', *J Physiol*, 505 (Pt 1): 65-76.

Herson, P. S., K. Lee, R. D. Pinnock, J. Hughes, and M. L. Ashford. 1999. 'Hydrogen peroxide induces intracellular calcium overload by activation of a non-selective cation channel in an insulin-secreting cell line', *J Biol Chem*, 274: 833-41.

Hess, B., B. Bekker, H.J.C. Berendsen, and J.G.E.M. Fraaije. 1997. 'LINCS: A linear constraint solver for molecular simulations', *Journal of Computatonal Chemistry*, 18: 1463-72.

Hill, K., S. McNulty, and A. D. Randall. 2004. 'Inhibition of TRPM2 channels by the antifungal agents clotrimazole and econazole', *Naunyn Schmiedebergs Arch Pharmacol*, 370: 227-37.

Hill, M. D., R. H. Martin, D. Mikulis, J. H. Wong, F. L. Silver, K. G. Terbrugge, G. Milot, W. M. Clark, R. L. Macdonald, M. E. Kelly, M. Boulton, I. Fleetwood, C. McDougall, T. Gunnarsson, M. Chow, C. Lum, R. Dodd, J. Poublanc, T. Krings, A. M. Demchuk, M. Goyal, R. Anderson, J. Bishop, D. Garman, M. Tymianski, and Enact trial investigators. 2012. 'Safety and efficacy of NA-1 in patients with iatrogenic stroke after endovascular aneurysm repair (ENACT): a phase 2, randomised, double-blind, placebo-controlled trial', *Lancet Neurol*, 11: 942-50.

Hoffman, N. E., B. A. Miller, J. Wang, J. W. Elrod, S. Rajan, E. Gao, J. Song, X. Q. Zhang, I. Hirschler-Laszkiewicz, S. Shanmughapriya, W. J. Koch, A. M. Feldman, M. Madesh, and J. Y. Cheung. 2015. 'Ca(2)(+) entry via Trpm2 is essential for cardiac myocyte bioenergetics maintenance', *Am J Physiol Heart Circ Physiol*, 308: H637-50.

Hooft, R. W., G. Vriend, C. Sander, and E. E. Abola. 1996. 'Errors in protein structures', *Nature*, 381: 272.

Huang, Y., P. A. Winkler, W. Sun, W. Lu, and J. Du. 2018. 'Architecture of the TRPM2 channel and its activation mechanism by ADP-ribose and calcium', *Nature*, 562: 145-49.

Inamura, K., Y. Sano, S. Mochizuki, H. Yokoi, A. Miyake, K. Nozawa, C. Kitada, H. Matsushime, and K. Furuichi. 2003. 'Response to ADP-ribose by activation of TRPM2 in the CRI-G1 insulinoma cell line', *J Membr Biol*, 191: 201-7.

Iordanov, I., C. Mihalyi, B. Toth, and L. Csanady. 2016. 'The proposed channel-enzyme transient receptor potential melastatin 2 does not possess ADP ribose hydrolase activity', *Elife*, 5.

Jakalian, A., D. B. Jack, and C. I. Bayly. 2002. 'Fast, efficient generation of high-quality atomic charges. AM1-BCC model: II. Parameterization and validation', *J Comput Chem*, 23: 1623-41.

Jang, Y., S. H. Lee, B. Lee, S. Jung, A. Khalid, K. Uchida, M. Tominaga, D. Jeon, and U. Oh. 2015. 'TRPM2, a Susceptibility Gene for Bipolar Disorder, Regulates Glycogen Synthase Kinase-3 Activity in the Brain', *J Neurosci*, 35: 11811-23.

Kraft, R., C. Grimm, K. Grosse, A. Hoffmann, S. Sauerbruch, H. Kettenmann, G. Schultz, and C. Harteneck. 2004. 'Hydrogen peroxide and ADP-ribose induce TRPM2-mediated calcium influx and cation currents in microglia', *Am J Physiol Cell Physiol*, 286: C129-37.

Krieger, E., T. Darden, S. B. Nabuurs, A. Finkelstein, and G. Vriend. 2004. 'Making optimal use of empirical energy functions: force-field parameterization in crystal space', *Proteins*, 57: 678-83.

Krieger, E., R. L. Dunbrack, Jr., R. W. Hooft, and B. Krieger. 2012. 'Assignment of protonation states in proteins and ligands: combining pKa prediction with hydrogen bonding network optimization', *Methods Mol Biol*, 819: 405-21.

Krieger, E., K. Joo, J. Lee, J. Lee, S. Raman, J. Thompson, M. Tyka, D. Baker, and K. Karplus. 2009. 'Improving physical realism, stereochemistry, and side-chain accuracy in homology modeling: Four approaches that performed well in CASP8', *Proteins*, 77 Suppl 9: 114-22.

Krieger, E., G. Koraimann, and G. Vriend. 2002. 'Increasing the precision of comparative models with YASARA NOVA--a self-parameterizing force field', *Proteins*, 47: 393-402.

Krieger, E., J. E. Nielsen, C. A. Spronk, and G. Vriend. 2006. 'Fast empirical pKa prediction by Ewald summation', *J Mol Graph Model*, 25: 481-6.

Krieger, E., and G. Vriend. 2015. 'New ways to boost molecular dynamics simulations', *J Comput Chem*, 36: 996-1007.

Kuhn, F. J., and A. Luckhoff. 2004. 'Sites of the NUDT9-H domain critical for ADP-ribose activation of the cation channel TRPM2', *J Biol Chem*, 279: 46431-7.

Lalatsa, A., A. G. Schatzlein, and I. F. Uchegbu. 2014. 'Strategies to deliver peptide drugs to the brain', *Mol Pharm*, 11: 1081-93.

Lange, I., S. Yamamoto, S. Partida-Sanchez, Y. Mori, A. Fleig, and R. Penner. 2009. 'TRPM2 functions as a lysosomal Ca2+-release channel in beta cells', *Sci Signal*, 2: ra23.

Li, L., R. Chen, and Z. Weng. 2003. 'RDOCK: refinement of rigid-body protein docking predictions', *Proteins*, 53: 693-707.

Li, X., and L. H. Jiang. 2019. 'A critical role of the transient receptor potential melastatin 2 channel in a positive feedback mechanism for reactive oxygen species-induced delayed cell death', *J Cell Physiol*, 234: 3647-60.

Maier, J. A., C. Martinez, K. Kasavajhala, L. Wickstrom, K. E. Hauser, and C. Simmerling. 2015. 'ff14SB: Improving the Accuracy of Protein Side Chain and Backbone Parameters from ff99SB', *J Chem Theory Comput*, 11: 3696-713.

McHugh, D., R. Flemming, S. Z. Xu, A. L. Perraud, and D. J. Beech. 2003. 'Critical intracellular Ca2+ dependence of transient receptor potential melastatin 2 (TRPM2) cation channel activation', *J Biol Chem*, 278: 11002-6.

Olah, M. E., M. F. Jackson, H. Li, Y. Perez, H. S. Sun, S. Kiyonaka, Y. Mori, M. Tymianski, and J. F. MacDonald. 2009. 'Ca2+-dependent induction of TRPM2 currents in hippocampal neurons', *J Physiol*, 587: 965-79.

Ostapchenko, V. G., M. Chen, M. S. Guzman, Y. F. Xie, N. Lavine, J. Fan, F. H. Beraldo, A. C. Martyn, J. C. Belrose, Y. Mori, J. F. MacDonald, V. F. Prado, M. A. Prado, and M. F. Jackson. 2015. 'The Transient Receptor Potential Melastatin 2 (TRPM2) Channel Contributes to beta-Amyloid Oligomer-Related Neurotoxicity and Memory Impairment', *J Neurosci*, 35: 15157-69.

Park, Y. R., J. N. Chun, I. So, H. J. Kim, S. Baek, J. H. Jeon, and S. Y. Shin. 2016. 'Data-driven Analysis of TRP Channels in Cancer: Linking Variation in Gene Expression to Clinical Significance', *Cancer Genomics Proteomics*, 13: 83-90.

Perraud, A. L., A. Fleig, C. A. Dunn, L. A. Bagley, P. Launay, C. Schmitz, A. J. Stokes, Q. Zhu, M. J. Bessman, R. Penner, J. P. Kinet, and A. M. Scharenberg. 2001. 'ADP-ribose gating of the calcium-permeable LTRPC2 channel revealed by Nudix motif homology', *Nature*, 411: 595-9.

Perraud, A. L., B. Shen, C. A. Dunn, K. Rippe, M. K. Smith, M. J. Bessman, B. L. Stoddard, and A. M. Scharenberg. 2003. 'NUDT9, a member of the Nudix hydrolase family, is an evolutionarily conserved mitochondrial ADP-ribose pyrophosphatase', *J Biol Chem*, 278: 1794-801.

Perraud, A. L., C. L. Takanishi, B. Shen, S. Kang, M. K. Smith, C. Schmitz, H. M. Knowles, D. Ferraris, W. Li, J. Zhang, B. L. Stoddard, and A. M. Scharenberg. 2005. 'Accumulation of free ADP-ribose from mitochondria mediates oxidative stress-induced gating of TRPM2 cation channels', *J Biol Chem*, 280: 6138-48.

Pierce, B., and Z. Weng. 2007. 'ZRANK: reranking protein docking predictions with an optimized energy function', *Proteins*, 67: 1078-86.

Rizzuti, M., M. Nizzardo, C. Zanetta, A. Ramirez, and S. Corti. 2015. 'Therapeutic applications of the cell-penetrating HIV-1 Tat peptide', *Drug Discov Today*, 20: 76-85.

Rueden, C. T., J. Schindelin, M. C. Hiner, B. E. DeZonia, A. E. Walter, E. T. Arena, and K. W. Eliceiri. 2017. 'ImageJ2: ImageJ for the next generation of scientific image data', *BMC Bioinformatics*, 18: 529.

Ryan, K., D. S. Backos, P. Reigan, and M. Patel. 2012. 'Post-translational oxidative modification and inactivation of mitochondrial complex I in epileptogenesis', *J Neurosci*, 32: 11250-8.

Shen, B. W., A. L. Perraud, A. Scharenberg, and B. L. Stoddard. 2003. 'The crystal structure and mutational analysis of human NUDT9', *J Mol Biol*, 332: 385-98.

Shimizu, T., R. M. Dietz, I. Cruz-Torres, F. Strnad, A. K. Garske, M. Moreno, V. R. Venna, N. Quillinan, and P. S. Herson. 2016. 'Extended therapeutic window of a novel peptide inhibitor of TRPM2 channels following focal cerebral ischemia', *Exp Neurol*, 283: 151-6.

Shimizu, T., T. A. Macey, N. Quillinan, J. Klawitter, A. L. Perraud, R. J. Traystman, and P. S. Herson. 2013. 'Androgen and PARP-1 regulation of TRPM2 channels after ischemic injury', *J Cereb Blood Flow Metab*, 33: 1549-55.

Smith, M. A., P. S. Herson, K. Lee, R. D. Pinnock, and M. L. Ashford. 2003. 'Hydrogen-peroxide-induced toxicity of rat striatal neurones involves activation of a non-selective cation channel', *J Physiol*, 547: 417-25.

Smith, N., L. Bornikova, L. Noetzli, H. Guglielmone, S. Minoldo, D. S. Backos, L. Jacobson, C. D. Thornburg, M. Escobar, T. C. White-Adams, A. S. Wolberg, M. Manco-Johnson, and J. Di Paola. 2018. 'Identification and characterization of novel mutations implicated in congenital fibrinogen disorders', *Res Pract Thromb Haemost*, 2: 800-11.

Starkus, J. G., P. Poerzgen, K. Layugan, K. G. Kawabata, J. I. Goto, S. Suzuki, G. Myers, M. Kelly, R. Penner, A. Fleig, and F. D. Horgen. 2017. 'Scalaradial Is a Potent Inhibitor of Transient Receptor Potential Melastatin 2 (TRPM2) Ion Channels', *J Nat Prod*, 80: 2741-50.

Tan, C. H., and P. A. McNaughton. 2016. 'The TRPM2 ion channel is required for sensitivity to warmth', *Nature*, 536: 460-3.

Tong, Q., W. Zhang, K. Conrad, K. Mostoller, J. Y. Cheung, B. Z. Peterson, and B. A. Miller. 2006. 'Regulation of the transient receptor potential channel TRPM2 by the Ca2+ sensor calmodulin', *J Biol Chem*, 281: 9076-85.

Toth, B., and L. Csanady. 2012. 'Pore collapse underlies irreversible inactivation of TRPM2 cation channel currents', *Proc Natl Acad Sci U S A*, 109: 13440-5.

Toth, B., I. Iordanov, and L. Csanady. 2015. 'Ruling out pyridine dinucleotides as true TRPM2 channel activators reveals novel direct agonist ADP-ribose-2'-phosphate', *J Gen Physiol*, 145: 419-30.

Verma, S., N. Quillinan, Y. F. Yang, S. Nakayama, J. Cheng, M. H. Kelley, and P. S. Herson. 2012. 'TRPM2 channel activation following in vitro ischemia contributes to male hippocampal cell death', *Neurosci Lett*, 530: 41-6.

Vriend, G. 1990. 'WHAT IF: a molecular modeling and drug design program', *J Mol Graph*, 8: 52-6, 29.

Wang, J., R. M. Wolf, J. W. Caldwell, P. A. Kollman, and D. A. Case. 2004. 'Development and testing of a general amber force field', *J Comput Chem*, 25: 1157-74.

Wang, L., T. M. Fu, Y. Zhou, S. Xia, A. Greka, and H. Wu. 2018. 'Structures and gating mechanism of human TRPM2', *Science*, 362.

Xu, D., and Y. Zhang. 2012. 'Ab initio protein structure assembly using continuous structure fragments and optimized knowledge-based force field', *Proteins*, 80: 1715-35.

Xu, D. and Y. Zhang. 2013. 'Toward optimal fragment generations for ab initio protein structure assembly', *Proteins*, 81: 229-39.

Yu, P., X. Xue, J. Zhang, X. Hu, Y. Wu, L. H. Jiang, H. Jin, J. Luo, L. Zhang, Z. Liu, and W. Yang. 2017. 'Identification of the ADPR binding pocket in the NUDT9 homology domain of TRPM2', *J Gen Physiol*, 149: 219-35.

Zhang, H., H. Liu, X. Luo, Y. Wang, Y. Liu, H. Jin, Z. Liu, W. Yang, P. Yu, L. Zhang, and L. Zhang. 2018. 'Design, synthesis and biological activities of 2,3-dihydroquinazolin-4(1H)-one derivatives as TRPM2 inhibitors', *Eur J Med Chem*, 152: 235-52.

Footnotes

This work was supported by the National Institutes of Health grants [T32GM007635] (Pharmacology training grant), and [R01NS092645] (to P.S.H).

Competing Interests

Patent pending.

Figure Legends:

Table 1. Description of peptides

Table 2. tatM2NX non-covalent interactions

*3 letter refers to amino acid; A: TRPM2; E: peptide

Figure 1. Molecular modeling of tatM2NX with the human TRPM2 channel NUDT9-H domain. A) Predicted secondary structure of tat-M2NX after MD-based refinement. The peptide is oriented N-term (left) to C-term (right). B) Top three predicted TPRM2-tatM2NX complexes, arrowhead indicates the human ADPR binding site within the NUDT9-H domain. C) Top scoring initial TPRM2-tatM2NX complex (left) and the same complex after 5ns of MD simulation (right).

Figure 2. The peptide tatM2NX inhibits TRPM2 currents in a concentration-dependent manner. A) Representative TRPM2 initial currents ($ADPR_i$, 3-4nA) activated by 100μM ADPR (red), with 2μM tatM2NX (black), or 20μM CTZ (gray). B) TRPM2 current density at 0.15-10μM tatM2NX compared to TRPM2 current at 0.05μM tatM2NX (ineffective concentration control). C) Dose-response curve showing normalized response (current density) vs. tatM2NX concentration. Potency was determined normalizing each concentration to TRPM2 current density with 0.05μM tatM2NX. All data represented as mean±SD and significance established at $p<0.05$ for $n\geq4$-7 (at least 3 experimental days/condition) using One-way ANOVA.

Molecular Pharmacology Fast Forward. Published on November 26, 2019 as DOI: 10.1124/mol.119.117549
This article has not been copyedited and formatted. The final version may differ from this version.

Figure 3. TatM2NX inhibits TRPM2-mediated GSK3β signaling and competes with ADPR to antagonize TRPM2. A) Co-immunoprecipitation of biotin-tagged tatM2NX with FLAG-tagged TRPM2 in doxycycline-inducible HEK293 cells (+Dox). No biotin-tatM2NX observed in un-induced cells (-Dox). At least 3 independent experimental days (n=3). B) Western blot of HEK293 cells expressing TRPM2 treated with 250μM H_2O_2 (+Con) compared to untreated cells (-Con) and cells pre-incubated with 2μM tatM2NX for 30min-4h followed by H_2O_2 stimulation (10min). C) $ADPR_f$ (control) currents with 500μM ADPR in the presence of 0 or 2μM tatM2NX. No significant differences in $ADPR_i$ for control and 2μM tatM2NX. All data is represented as mean±SD and significance established at $p<0.05$ for $n\geq4$ (at least 3 experimental days/condition) using Student's *t*-test, $ADPR_f$= final ADPR current, $ADPR_i$= initial ADPR current.

Figure 4. The C-terminus of tatM2NX is sufficient to antagonize TRPM2. A) TRPM2 current density in the presence of 2μM tat Cterm (blue), tatWV-AA (sky blue), or tat Nterm (green). All peptides were individually compared to control group ($ADPR_f$). B) Representative images for Ca^{2+} imaging experiments at Time 0min and 20min for 250μM H_2O_2 (control) or H_2O_2 + 2μM tatM2NX. Fluo5F, AM (5μM, green) is the fluorescent Ca^{2+} indicator. C) Quantification of changes in fluorescence/baseline fluorescence (F/F_0) for each peptide (2μM). TatM2NX and tat Cterm significantly inhibit TRPM2 activity in HEK293 cells. F/F_0, corresponding to TRPM2 activity, is inhibited by 20μM CTZ (positive control). D) Area under the curve (AUC) analysis for each peptide: H_2O_2 control (black), tatM2NX (red), tat Cterm (blue), tatWV-AA (sky blue), tat Nterm (green). tatM2NX, tat Cterm, and CTZ significantly decreased AUC for TRPM2 activity, while tatWV-AA significantly increased AUC. All data is represented as mean±SD and significance established as $p<0.05$ using One-way ANOVA with Dunnett's post-hoc for multiple group comparison, $n\geq4$-10 for electrophysiology and $n\geq25$-53 cells for Ca^{2+} imaging (4-6 independent experiments).

Molecular Pharmacology Fast Forward. Published on November 26, 2019 as DOI: 10.1124/mol.119.117549
This article has not been copyedited and formatted. The final version may differ from this version.

Table 1. Description of peptides

Peptide	Concentration	Description
TatM2NX	0.05-10μM	Cell permeable, parent peptide YGRKKRRQRRRGSREPGEMLPR KLKRVLRQEFWV
TatWV-AA	2μM	Parent peptide, residues mutated to Alanine YGRKKRRQRRRGSREPGEMLPR KLKRVLRQEFAA
Tat Cterm	2μM	Truncated peptide YGRKKRRQRRRKLKRVLRQEFWV
Tat Nterm	2μM	Truncated peptide YGRKKRRQRRRGSREPGEMLPR

Molecular Pharmacology Fast Forward. Published on November 26, 2019 as DOI: 10.1124/mol.119.117549
This article has not been copyedited and formatted. The final version may differ from this version.

Table 2. tatM2NX non-covalent interactions

Interaction (A=TPRM2, E=Peptide)	Interaction Category	Interaction Type
A:ARG1280:HH21 - E:GLU31:OE1	Hydrogen Bond; Electrostatic	Salt Bridge; Attractive Charge
A:ARG1433:HH12 - E:VAL34:OXT	Hydrogen Bond; Electrostatic	Salt Bridge; Attractive Charge
A:ARG1433:HH22 - E:VAL34:OXT	Hydrogen Bond; Electrostatic	Salt Bridge; Attractive Charge
A:LYS1401:NZ - E:VAL34:O	Electrostatic	Attractive Charge
A:ARG1433:NH1 - E:GLU31:OE2	Electrostatic	Attractive Charge
A:ARG1433:NH2 - E:VAL34:O	Electrostatic	Attractive Charge
E:ARG9:NH2 - A:GLU121:OE2	Electrostatic	Attractive Charge
A:TYR1349:HH - E:VAL34:OXT	Hydrogen Bond	Conventional Hydrogen Bond
A:LEU1381:H - E:GLN30:OE1	Hydrogen Bond	Conventional Hydrogen Bond
A:SER1382:H - E:GLN30:OE1	Hydrogen Bond	Conventional Hydrogen Bond
A:GLY1389:H - E:PHE32:O	Hydrogen Bond	Conventional Hydrogen Bond
A:SER1391:HG - E:GLU31:O	Hydrogen Bond	Conventional Hydrogen Bond
A:SER1391:HG - E:VAL34:O	Hydrogen Bond	Conventional Hydrogen Bond
A:LYS1401:HZ3 - E:GLU31:O	Hydrogen Bond	Conventional Hydrogen Bond
A:HIS1488:HE2 - E:TRP33:O	Hydrogen Bond	Conventional Hydrogen Bond
E:ARG6:HE - A:PHE108:O	Hydrogen Bond	Conventional Hydrogen Bond
E:ARG6:HH21 - A:PHE108:O	Hydrogen Bond	Conventional Hydrogen Bond
E:LYS23:HZ1 - A:PRO1248:O	Hydrogen Bond	Conventional Hydrogen Bond
E:LYS23:HZ2 - A:ASN1249:O	Hydrogen Bond	Conventional Hydrogen Bond
E:GLN30:HE21 - A:SER1382:OG	Hydrogen Bond	Conventional Hydrogen Bond
A:HIS106:HD2 - E:TYR1:OH	Hydrogen Bond	Carbon Hydrogen Bond
A:GLY110:HA1 - E:TYR1:OH	Hydrogen Bond	Carbon Hydrogen Bond
A:PRO1380:HD1 - E:GLN30:OE1	Hydrogen Bond	Carbon Hydrogen Bond
A:SER1382:HB1 - E:GLN30:OE1	Hydrogen Bond	Carbon Hydrogen Bond
A:SER1391:HB2 - E:VAL34:O	Hydrogen Bond	Carbon Hydrogen Bond
A:SER1391:HB2 - E:VAL34:OXT	Hydrogen Bond	Carbon Hydrogen Bond
E:ARG3:HA - A:GLN109:OE1	Hydrogen Bond	Carbon Hydrogen Bond

E:LYS23:HE1 - A:PRO1248:O	Hydrogen Bond	Carbon Hydrogen Bond
E:LYS23:HE1 - A:ASN1249:O	Hydrogen Bond	Carbon Hydrogen Bond
E:ARG26:HD1 - A:LEU1381:O	Hydrogen Bond	Carbon Hydrogen Bond
A:CYS1250 - E:LEU20	Hydrophobic	Alkyl
E:ARG26 - A:LEU1381	Hydrophobic	Alkyl
A:PHE108 - E:ARG6	Hydrophobic	Pi-Alkyl
A:HIS1488 - E:VAL34	Hydrophobic	Pi-Alkyl
E:PHE32 - A:ARG1404	Hydrophobic	Pi-Alkyl
E:PHE32 - A:ILE1405	Hydrophobic	Pi-Alkyl
E:TRP33 - A:PRO1380	Hydrophobic	Pi-Alkyl
E:TRP33 - A:VAL1377	Hydrophobic	Pi-Alkyl
E:TRP33 - A:PRO1380	Hydrophobic	Pi-Alkyl

*3 letter refers to amino acid; A: TRPM2; E: peptide

Molecular Pharmacology Fast Forward. Published on November 26, 2019 as DOI: 10.1124/mol.119.117549
This article has not been copyedited and formatted. The final version may differ from this version.

Figure 1.

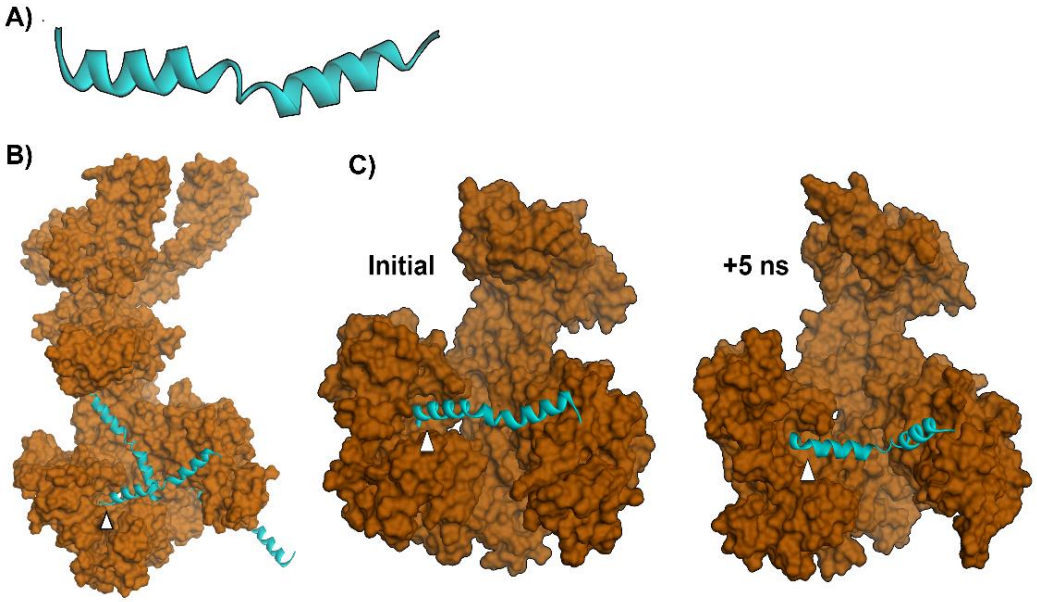

Molecular Pharmacology Fast Forward. Published on November 26, 2019 as DOI: 10.1124/mol.119.117549
This article has not been copyedited and formatted. The final version may differ from this version.

Figure 2.

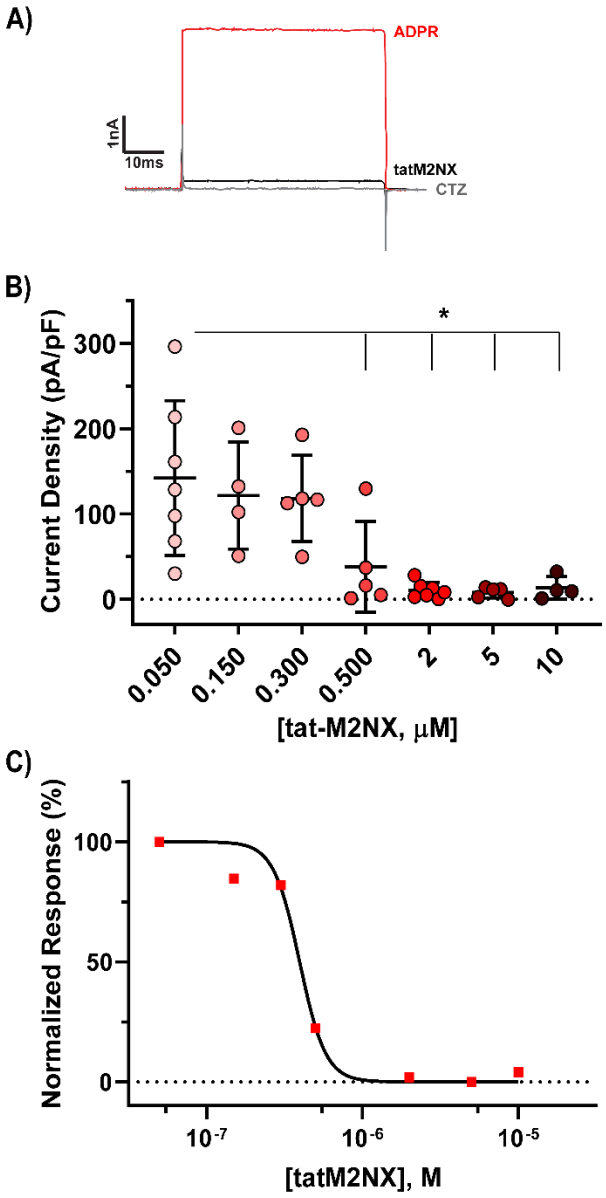

Molecular Pharmacology Fast Forward. Published on November 26, 2019 as DOI: 10.1124/mol.119.117549
This article has not been copyedited and formatted. The final version may differ from this version.

Figure 3.

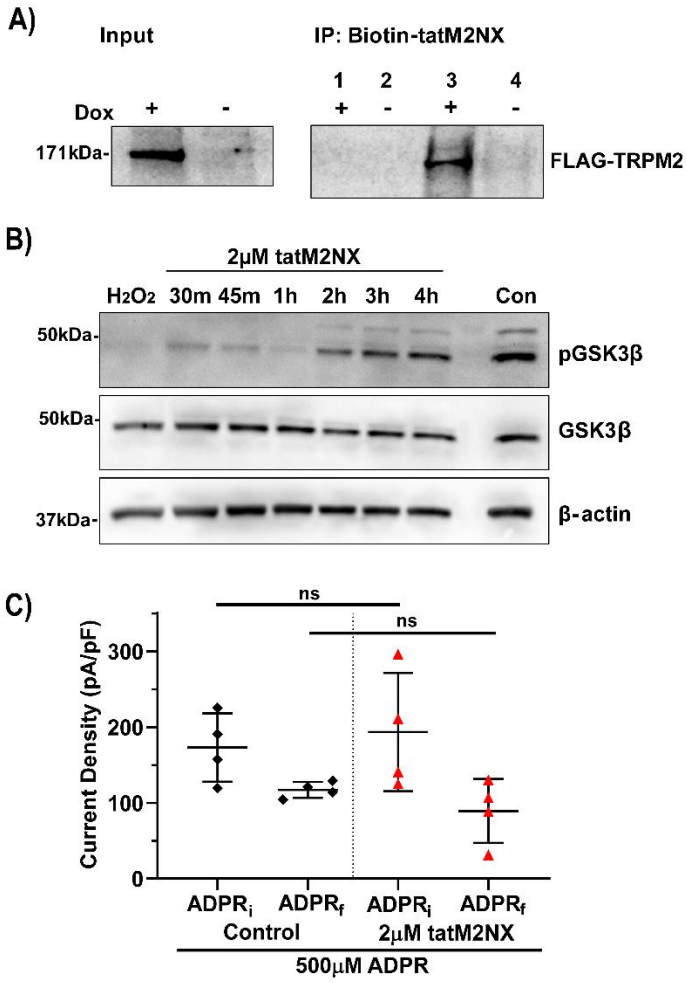

Molecular Pharmacology Fast Forward. Published on November 26, 2019 as DOI: 10.1124/mol.119.117549
This article has not been copyedited and formatted. The final version may differ from this version.

Figure 4.